The magnetic properties of Er/Lu superlattices

1997 J. Phys.: Condens. Matter 9 8693

(http://iopscience.iop.org/0953-8984/9/41/015)

J. Phys.: Condens. Matter **9** (1997) 8693–8705. Printed in the UK PII: S0953-8984(97)84041-6

The magnetic properties of Er/Lu superlattices

J A Simpson†, R A Cowley†, R C C Ward†, M R Wells† and D F McMorrow‡

† Oxford Physics, Clarendon Laboratory, Parks Road, Oxford, UK
‡ Department of Solid State Physics, Risø National Laboratory, DK-4000, Roskilde, Denmark

Received 7 May 1997, in final form 17 July 1997

Abstract. Superlattices of erbium and lutetium were grown by molecular beam epitaxy (MBE) and were examined using x-ray and neutron scattering techniques. When cooled below a temperature of about 86 K, the superlattices develop a coherent longitudinal modulated magnetic structure similar to that found in bulk Er. The structures are coherent over approximately 600 Å, or several superlattice block lengths. When cooled below 65 K, the Er moments also order in the basal plane and form a cycloidal structure for which the coherence length decreases to about 200 Å. At low temperatures, below 20 K, the cone structure of bulk Er is suppressed and the structure of the Er blocks in the superlattice is a commensurate, $\boldsymbol{q} = \frac{1}{4}\boldsymbol{c}^*$, cycloid. These results are compared with those obtained for bulk Er and for Er/Y superlattices for which the basal-plane strain is of the opposite sign to that of Er/Lu superlattices.

1. Introduction

Many studies of rare-earth based superlattices (SLs) have been on systems formed by the sequential deposition of a magnetic material and a non-magnetic spacer. For the heavy rare earths, the magnetic structure is modulated along the *c*-axis, which is also normally the growth direction of the SL. The Dy/Y [1], Gd/Y [2], Er/Y [3], Ho/Y [4], Dy/Lu [5] and Ho/Lu [6] systems have been studied. The most intriguing feature of the magnetic properties is the observation of coherence in the magnetic ordering between adjacent blocks of the SL. For example, in the Ho/Y system, the phase and chirality of the Ho helix is coherent across several blocks and there is an effective phase advance of the helix across the nominally non-magnetic Y layers. This coherence is maintained over a length of typically 500–1000 Å for SLs in which the non-magnetic layers have a thickness of between 50 and 100 Å.

A theoretical treatment of the coherence of the magnetic order found in the rare-earth SLs was first considered by Yafet [7]. In the conventional RKKY theory of the exchange in metallic systems, a 4f localized moment spin polarizes the conduction electrons (5d, 6s), which then gain a small magnetization of the same form as that of the ordered moments. These conduction electrons travel through the material, subsequently interacting with other 4f moments. In a SL, the spins at the edge of a magnetic block polarize the conduction electrons in the non-magnetic spacer. This polarization propagates through the non-magnetic block as determined by the conduction electron susceptibility. Since the conduction electron susceptibilities of Y and Lu both have peaks at non-zero wave vectors

0953-8984/97/418693+13$19.50

along the crystallographic c-axis (similar to the magnetic heavy rare earths [8]), a spin-density wave develops in the non-magnetic region, which, it is suggested, induces the coupling between neighbouring magnetic blocks.

Another important influence on the magnetic properties of a SL is the strain imposed by the clamping of the SL to the substrate. This alters the properties in two ways. Firstly the c lattice parameter of a SL can vary freely, but the a lattice parameter is clamped at some average value intermediate between that of the two constituents of the SL. The c/a-ratio for the magnetic layers may then be different from that of the bulk. Andrianov [9] has suggested that in the bulk rare earths the helical turn angle is correlated with the c/a-ratio, and that for $c/a > 1.582$ the stable structure is ferromagnetic; therefore any change in the c/a-ratio can be expected to alter the properties of the SL. This suggestion is consistent with the result that, while bulk Dy has a basal-plane ferromagnetic structure below 79 K, Dy/Y SLs [1] (expansive basal-plane strain and reduced c/a) have helical structures at all temperatures and Dy/Lu SLs [5] (compressive basal-plane strain and increased c/a) have a ferromagnetic transition above 79 K.

The second effect is that the clamping of the SL by the substrate prohibits a basal-plane strain occurring in response to the development of a ferromagnetic structure, and hence the relative energies of the different structures may be altered. This may account partially for why some Ho/Lu SLs [6] develop a basal-plane ferromagnetic structure at low temperatures rather than the cone structure found for bulk Ho. In contrast, both effects probably contribute to the suppression of the cone phase for Ho/Y SLs [4].

Erbium has the most complex magnetic behaviour of all the heavy rare-earth elements, and an understanding of the magnetic structures has developed gradually over the last 30 years. The first thorough study was performed by Cable *et al* [10], who observed three different magnetic structures. Below the Néel temperature $T_N = 84$ K, the ordered magnetic moments align along the c-axis in a sinusoidally modulated structure. Further cooling causes the wave vector to increase slightly and the structure 'squares up' and shows higher harmonics in the diffraction patterns. Below $T_N' = 52$ K, the magnetic moments also order in the basal-plane forming a cycloidal structure in which the moments lie on an ellipse in the a–c plane [11]. Gibbs *et al* [12] used high-resolution x-ray magnetic scattering to show that the wave vector locks in to a series of discrete values below 50 K with values of $\frac{2}{7}\boldsymbol{c}^*$, $\frac{3}{11}\boldsymbol{c}^*$, $\frac{4}{15}\boldsymbol{c}^*$ etc until reaching $\frac{1}{4}\boldsymbol{c}^*$ at 24 K, where $\boldsymbol{c}^*$ is the reciprocal lattice vector parallel to the c-axis. These long-period magnetic structures occur because of the competition between the crystal field and exchange interactions. Below a temperature of 18 K, the moments form a cone structure similar to that of bulk Ho with the angle between the moments and the c-axis about 30°, and the wave vector $\boldsymbol{q} = \frac{5}{21}\boldsymbol{c}^*$. This phase is stabilized by a combination of the dipolar forces and the magnetoelastic energy [13]. Further experiments [11] have clarified the nature of the commensurable structures formed in the cycloidal phase, and have shown that two-ion couplings of trigonal symmetry produce distortions of the planar cycloidal phase.

The properties of Er/Y SLs have been studied by Borchers *et al* [3], who showed that the magnetic structures were coherent between the different Er blocks and that both T_N and T_N' were lower than for bulk Er, while the transition to the cone phase did not occur. Borchers *et al* suggested that these differences from the behaviour of the bulk arise because of the strain of the Er blocks in the SLs. The a lattice parameter of Y is 2.5% larger than that of Er whereas that of Lu is 1.2% smaller. Consequently a study of Er/Lu SLs enables the effect of strain on the properties of the SLs to be investigated further. In section 2 we describe the growth and characterization of the Er/Lu SLs, while in section 3 the neutron scattering results and the magnetic structures of the SLs are discussed. These results are

compared with those for other rare-earth SLs and discussed in the light of current theory in section 4.

2. Sample growth and characterization

The Er/Lu SLs were grown by the technique of molecular beam epitaxy (MBE) and details of the growth facility in Oxford and the procedure used have been given before [4]. The sapphire substrates were cleaned and heated to a temperature of 1200 °C and a layer of Nb (500 Å) deposited to form a chemical barrier. A seed layer of 1000 Å of Lu was then deposited with the growth direction corresponding to the hexagonal *c*-axis. The substrate temperature was reduced to 400 °C for the growth of the Lu seed and the SL which was grown by alternately depositing Lu and Er and repeating the process 40 times. Finally a 200 Å Lu cap was grown on top of the SL to protect it from oxidation. The crystalline quality of the SL was monitored during the growth process by RHEED.

The samples were characterized, *ex situ*, by high-resolution x-ray scattering using a triple-crystal diffractometer mounted on a Stoe rotating anode generator operating at 6 kW. The wave-vector transfer was scanned along the SL [00*l*] direction around the (002) Bragg peak of bulk Er. The intensity observed for the SL $Er_{30}Lu_{10}$ is shown in figure 1, where the notation indicates that the SL repeating unit nominally consists of 30 planes of Er and 10 planes of Lu.

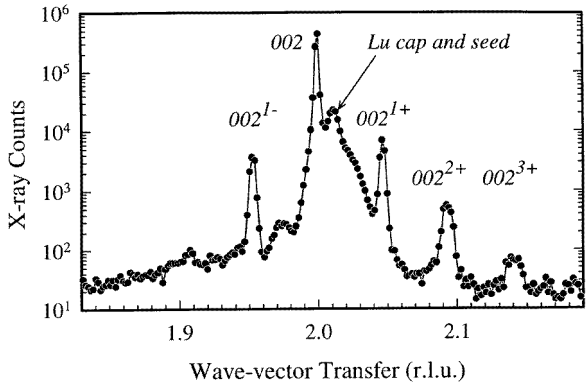

Figure 1. The x-ray scattering observed when the wave-vector transfer was scanned along the [00*l*] direction for the $Er_{30}Lu_{10}$ sample. The sharp peaks arise from the superlattice and in addition there is a peak from the Lu seed and cap.

Figure 1 shows a series of peaks with a constant separation in wave-vector and the jth superlattice peak with a wave-vector transfer below the (002) reflection is denoted as (002^{j-}) and similarly (002^{j+}) is the corresponding peak at wave-vector transfers larger than (002). The separation of these peaks gives the superlattice repeat distance and hence the number of atomic planes of the repeating unit as listed in table 1.

The wave-vector transfer was also scanned transversely through the peaks shown in figure 1 to measure the mosaic spread which was found to be about 0.14°, significantly smaller than for most rare-earth SLs and smaller than for Er/Y SLs [3] for which the mosaic spread was typically 0.3°. This may be because the lattice mismatch between Er and Lu is less than that between Er and Y.

Table 1. Structure of Er/Lu superlattices.

Nominal structure	Bilayer planes	Erbium planes	Lutetium planes	Mosaic spread (°)
$Er_{30}Lu_{10}$	42	29	13	0.14
$Er_{20}Lu_{20}$	39	20	19	0.13
$Er_{20}Lu_{10}$	29	20	9	0.15
$Er_{10}Lu_{10}$	21	10.5	10.5	0.14

The interfaces between the Er and Lu are on average not sharp but broadened by interface roughness and by diffusion, and modelling [14] suggests that they typically have a width of 3–4 atomic planes. Figure 1 shows also that the (002^{3+}) peak is broader than the most intense (002) peak showing that the position of the interfaces is somewhat random [14].

The neutron scattering experiments were performed at the DR3 reactor of Risø National Laboratory, Denmark, using the triple-axis spectrometers TAS1 and TAS6. The samples were mounted with the $[h0l]$ crystallographic plane in the scattering plane and a closed cycle cryostat was used to control the temperature to ± 0.1 K. The incident neutron energy was 5 meV and a cooled Be filter was used to suppress higher-order contaminant neutrons from the monochromator. The collimation was chosen to give an in-plane wave-vector resolution of typically 0.01 r.l.u. for elastically scattered neutrons. The scattered intensity was measured while the wave-vector transfer, $\boldsymbol{Q}$, was varied along the $[00l]$ and $[10l]$ reciprocal lattice directions. The results for the former scans give information about the ordered moments in the basal-plane while the latter scans provide information about both the basal-plane and c-axis components. The c and a lattice parameters were measured at low temperatures and the ratio for c/a was 1.5756 ± 0.0020 for all the SLs.

3. Magnetic structures

It is convenient to divide the discussion of the magnetic structures into several parts: firstly temperatures below T_N but above T_N', when the structure is similar to the longitudinally modulated structure of bulk Er; secondly the region below T_N' for which the ordering of the magnetic moments is in both the longitudinal direction and the basal plane; thirdly, the coherence length of the structures and then lastly the models which have been fitted to the experimental results.

3.1. The longitudinally modulated phase

For temperatures just below T_N, temperature dependent magnetic scattering is observed for scans of the wave-vector transfer, $\boldsymbol{Q}$, along the $[10l]$ direction but not for similar scans along $[00l]$. A typical illustration is shown in figure 2 which shows the scattering observed at 70 K from the $Er_{20}Lu_{10}$ sample. The nuclear scattering is independent of temperature and is labelled N while the magnetic scattering is labelled M. The absence of any magnetic scattering for wave-vector transfers along $[00l]$ shows that in this phase the ordered magnetic moments are aligned along the c-axis as found for bulk Er at these temperatures. The magnetic scattering from all of the SLs in this phase consists of a series of sharp peaks with a spacing the same as that observed in the x-ray scattering experiments, showing that the magnetic structure is coherent across several non-magnetic Lu blocks. The temperatures for the onset of the longitudinal modulated structure, T_N, were measured and are listed in table 2. The temperature tends to decrease as the thickness of the Er blocks is reduced.

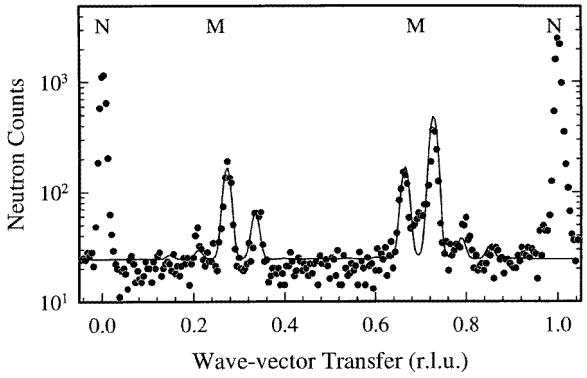

Figure 2. The neutron scattering from the $Er_{20}Lu_{10}$ sample at 70 K as the wave-vector transfer is varied along the [10*l*] direction. The peaks marked N are nuclear temperature independent scattering and those marked M are from magnetic scattering.

Table 2. Magnetic properties of Er/Lu superlattices at high temperatures.

Superlattice	T_N (K)	$q_{Er}(T_N)$ c^*	$q_{Lu}(T_N)$ c^*	T'_N (K)	$\xi(T_N)$ (Å)
$Er_{30}Lu_{10}$	85(3)	0.290(2)	0.240(2)	65(3)	542(50)
$Er_{20}Lu_{20}$	83(3)	0.290(2)	0.240(2)	65(3)	446(50)
$Er_{20}Lu_{10}$	75(3)	0.282(2)	0.242(2)	63(3)	493(50)
$Er_{10}Lu_{10}$	75(3)	0.290(2)	0.240(2)	53(3)	379(40)

Higher harmonics of the scattering are observed for bulk Er but these could not be clearly identified for the SLs because the first-order harmonics occur over a range of wave-vectors close to $\frac{1}{4}c^*$ so that the third and fifth harmonics then occur at very similar wave-vectors but associated with the next Bragg reflection.

3.2. The cycloidal phase

All of the SLs show magnetic scattering when the wave-vector transfer is scanned along the [00*l*] direction below a temperature of T'_N. The values of T'_N are listed in table 2 and with the exception of the $Er_{10}Lu_{10}$ sample are substantially higher than $T'_N = 52$ K of bulk Er. Two examples of the results at 10 K are shown in figure 3 for the $Er_{30}Lu_{10}$ sample and in figure 4 for the $Er_{20}Lu_{10}$ sample. The nuclear peaks are labelled by N and the magnetic peaks by M. None of the samples exhibit additional scattering at the (100) Bragg position at any temperature above 9 K. These results show that below T'_N the moments are ordered and modulated along both the *c*-axis and in the basal plane, while the cone phase, which is found for bulk Er below 18 K, either does not occur for the SLs or only occurs at a much lower temperature.

The corresponding phase for bulk Er forms a number of long-period structures which produce higher harmonics in the scattering, and the details of these structures could only be obtained by analysing these harmonics in detail [11]. One of the difficulties of studying the SLs is that the higher harmonics cannot be clearly identified as explained in section 3.1 because they all overlap as indicated in figure 3.

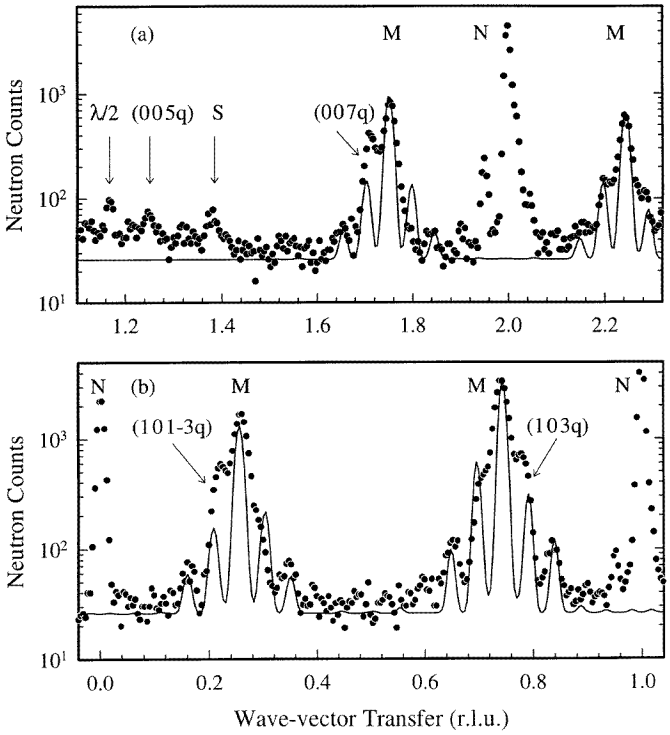

Figure 3. The neutron scattering from the $Er_{30}Lu_{10}$ sample at 10 K. The wave-vector transfer was varied along the [00*l*] (a) and [10*l*] (b) directions and N marks the nuclear scattering and M the magnetic peaks. The solid line shows a fit to the first harmonics of the modulated structure as described in the text. The positions of some of the higher harmonics are marked on the figure. The peak labelled $\lambda/2$ arises from $\lambda/2$ scattering from the sapphire substrate and that marked S is spurious and temperature independent.

3.3. The coherence length

The coherence length of the magnetic structures was determined from the widths of the peaks shown in figures 2–4. The profiles of the peaks with wave-vector transfer $\boldsymbol{Q}$ less than the (002) Bragg reflection or with $\boldsymbol{Q}$ close to the (100) Bragg reflection were fitted to a sum of three or four Gaussians with a constant separation and width. The widths (FWHM) obtained from these fits, σ_0, were corrected for the instrumental widths, σ_R, which were calculated as described by Cooper and Nathans [15]. The width arising from a Gaussian broadening of the magnetic peaks is then given by

$$\sigma = (\sigma_0^2 - \sigma_R^2)^{1/2}$$

and the coherence length is defined to be $\xi = 2\pi/\sigma$.

This procedure assumes that the broadening of the scattering has a Gaussian form. If it had an intrinsic Lorentzian form the coherence length would be different, but the qualitative behaviour would be the same.

The coherence lengths were obtained from the results using the procedure described above and are shown for the $Er_{30}Lu_{10}$ sample and for the $Er_{20}Lu_{10}$ sample in figure 5. The coherence lengths at T_N and at 10 K for all the samples are listed in tables 2 and 3. The scatter of the points in the figures indicates the random errors in the analysis, while the

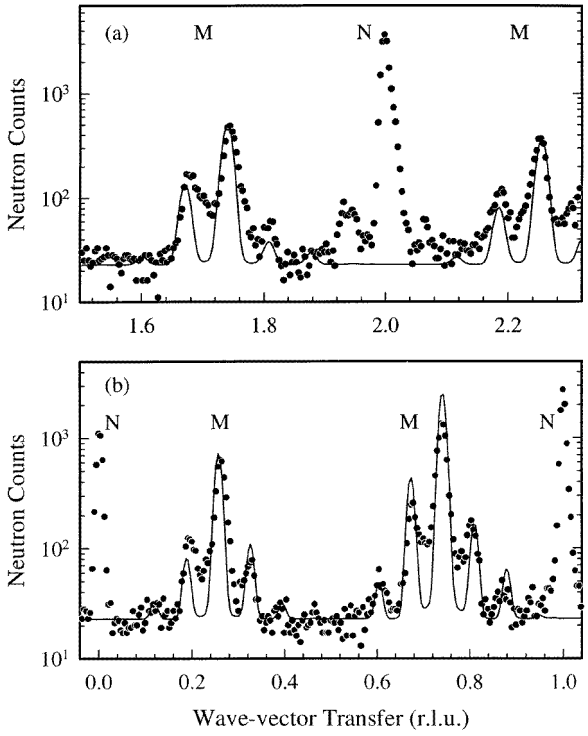

Figure 4. The neutron scattering from the $Er_{20}Lu_{10}$ sample at 10 K: (a) the scattering as the wave-vector transfer was varied along the [00*l*] and (b) the [10*l*] direction. The solid line is a fit to the first-harmonic model of the structure as described in the text.

Table 3. Magnetic properties of Er/Lu superlattices at 10 K.

Superlattice	q_{Er} c^*	q_{Lu} c^*	$\xi(10\ K)$ (Å)	r	$\Phi_c-\Phi_{bp}$ (°)
$Er_{30}Lu_{10}$	0.250(2)	0.273(2)	274(30)	0.3(1)	66(5)
$Er_{20}Lu_{20}$	0.250(2)		237(25)	0.9(1)	0(5)
$Er_{20}Lu_{10}$	0.250(2)		208(20)	0.4(1)	38(5)
$Er_{10}Lu_{10}$	0.250(2)	0.258(2)	207(20)	0.7(1)	49(5)

coherence lengths deduced from the (10*l*) data and the (00*l*) data are within error the same except possibly for one sample close to T_N'. For the longitudinally modulated phase, the coherence length is within error independent of temperature and varies between four and seven blocks of the SL with the largest value observed for the thinner Lu block lengths.

The coherence length of the cycloid decreases with decreasing temperature and is approximately the same for both the longitudinal and basal-plane ordering, and at low temperatures it has decreased to roughly one half that at T_N'. Most SLs of rare earths and non-magnetic metals have basal-plane helical magnetic structures and temperature independent correlation lengths, but similar temperature dependent results have been observed for Er/Y SLs [3], which also show both basal-plane and longitudinal ordering. A temperature dependence of the width of the scattering has been observed by high-resolution x-ray

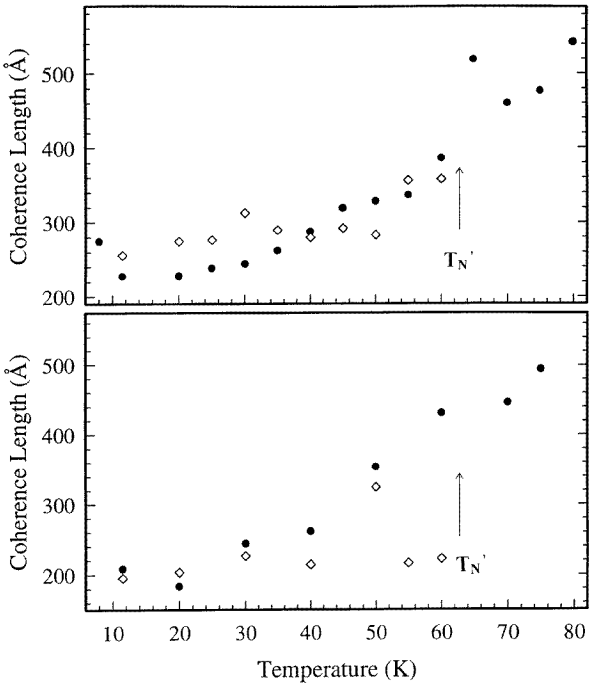

Figure 5. The temperature dependence of the magnetic coherence length for the $Er_{30}Lu_{10}$ (upper) and $Er_{20}Lu_{10}$ (lower) SLs. The filled points are from the [10*l*] data and the open points from the [00*l*] data. The spread of the points indicates the errors.

scattering measurements from a Ho film and discussed in terms of magneto-elastic coupling [16]. The increase in the widths observed in these experiments are about an order of magnitude larger than for the Ho film and the magneto-elastic effects could not have been measured in our experiments.

3.4. Models of the magnetic structures

The magnetic structures were analysed with a similar model to that used for the Ho/Y SLs [4]. Since it was not possible to observe the higher harmonics of the scattering, the Er moments were assumed to have an undistorted sinusoidal modulation which propagates coherently through the non-magnetic Lu layers. The wave vector describing the phase angle between the moments on successive Er planes is q_{Er} and the corresponding effective wave vector for the Lu is q_{Lu}. The corresponding lattice parameters are d_{Er} and d_{Lu}. The ordered magnetic moment on the lth plane is given by

$$\langle J_c(l)\rangle = A_c(l)\sin(q_l R_l) \qquad \langle J_{bp}(l)\rangle = A_{bp}(l)\cos(q_l R_l)$$

where R_l is the position, A_c and A_{bp} are the amplitudes of the ordered moments along the c-axis and in the basal-plane respectively and q_l is the wave-vector associated with the lth plane. These amplitudes were calculated by taking account of the width of the interfaces, λ, by weighting the properties of Er and Lu with a tanh function so that, for example, $A(l) = A(1 - \tanh((l - I)/(\lambda))$, where I is the position of the interface and A is the amplitude of the ordered moment in the Er blocks if the interfaces were sharp.

The magnetic structure factor for the scattering from an SL with a cycloidal structure can then be obtained if the plane of the cycloid is randomly distributed among the a-axes as

$$I(\boldsymbol{Q}) = [r^2(1 + Q_c^2/Q^2)/2 + (1 - Q_c^2/Q^2)][|A_+(Q)|^2 + |A_-(Q)|^2]$$

where Q_c is the component of $\boldsymbol{Q}$ along the c-axis, r is the ratio of the amplitude of the ordered Er moment between the basal-plane and c-axis components, $r = A_{bp}/A_c$, while

$$A_+(\boldsymbol{Q}) = \sum \langle J_c(l) \rangle \exp(\mathrm{i}(\boldsymbol{Q} + \boldsymbol{q}_l) \cdot \boldsymbol{R}_l)\ \delta(Q_c - n/D + \Phi/D)$$

where the summation is over one SL bilayer, D is the SL repeat distance and Φ is the total phase advance over one repeating block. The factorization of the structure factor depends on the first term being the same for each superlattice block. For the scattering along $[10l]$ the scattering is different for each of the two sub-lattices of the hexagonal unit cell, so that the second term in the sum can be factorized only if the number of planes in each block is even. Calculations were performed with blocks containing an odd number of planes and a half-integer number of planes by extending the sum in the first term to over two or four blocks.

The scattering was calculated by convoluting the expression for the structure factor with a Gaussian to describe the resolution of the instrument, including the resolution correction for the scan direction [17] and the form factor [18]. Fits were performed by varying d_{Er}, d_{Lu}, q_{Er}, q_{Lu}, λ and r in a least-squares fit routine to minimize χ^2. After the initial fits, d_{Er}, d_{Lu} and λ were held fixed for each sample and the other parameters were allowed to vary with temperature. Typical fits are shown by the solid lines in figures 2–4 and there is generally reasonable agreement between the model and the experimental results. The results are less satisfactory at low temperatures but this may well be due to the absence of the higher harmonics in the model.

The variation with temperature of the wave-vectors describing the phase angles for the $Er_{30}Lu_{10}$ and $Er_{10}Lu_{10}$ samples is shown in figure 6. For $T > T_N'$ the Er and Lu wave-vectors are constant and correspond to values of 0.282 and 0.239 respectively in units of $\boldsymbol{c}^*$. The small increase of q_{Er} found on cooling the bulk from T_N to T_N' is not observed for the SLs, and instead the wave-vector is within error constant at the commensurate value of $\frac{2}{7}\boldsymbol{c}^*$. For the temperature range between 20 K and T_N', q_{Er} decreases as observed for bulk Er, whilst the Lu phase angle increases. As described in section 3.2, the cone phase formed by bulk Er does not occur, and instead the Er moments lock in to form a commensurable long-period cycloidal structure with the wave-vector $\frac{1}{4}\boldsymbol{c}^*$. These values were obtained by combining the results of the modelling with a study of the higher harmonics along the $[00l]$ direction. Although this scattering is weak, the $(0\,0\,3q)$ and $(0\,0\,5q)$ peaks do not in this case overlap with the other scattering features, and so may be used to determine the Er wave vector directly. The $q = \frac{1}{4}\boldsymbol{c}^*$ structure is strongly favoured by the fourth-order crystal field anisotropy of Er, and is probably a (44) sequence of moments. This notation describes a period of eight atomic planes, in which the c components of the first four moments are aligned down the c-axis while the second four are aligned up this axis. In a study of the structure of bulk Er [11], it was not possible to determine whether this commensurate structure had the (44) or a (3030) configuration. In the latter case, the repeat of eight moments are grouped three down along c, then a single moment in the basal-plane, followed by three up and a final single moment in the basal-plane. This is also a possible magnetic structure for the SL.

The variation of the Lu wave-vector is different from that of previous studies of magnetic/Y rare-earth superlattices. In systems such as Ho/Y [4], the turn angle of the

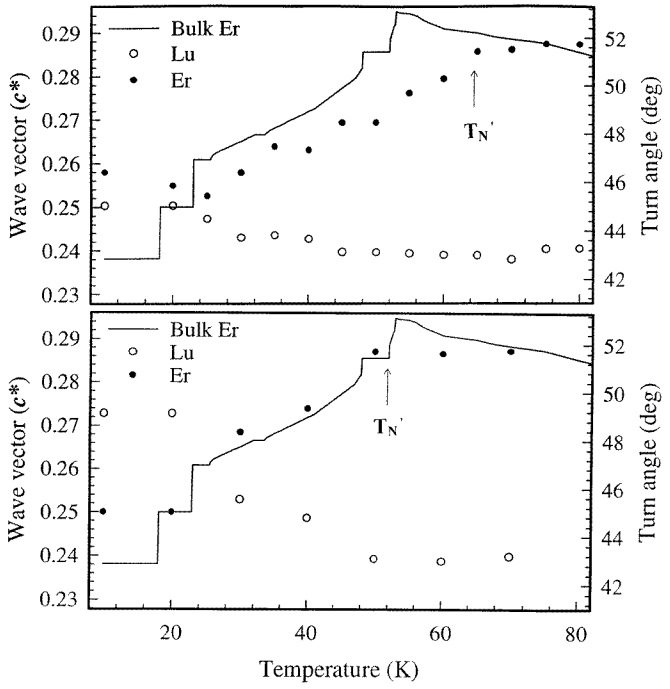

Figure 6. The variation of the Er and Lu wave-vectors (turn angles) for the $Er_{30}Lu_{10}$ (upper) and $Er_{10}Lu_{10}$ (lower) SLs. The solid line shows the variation for bulk Er.

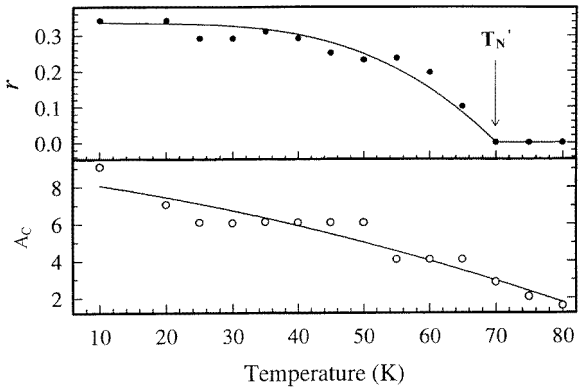

Figure 7. The temperature dependence of amplitude of the longitudinal ordering A_c and the ratio of the amplitudes of the transverse to longitudinal ordering, r, for the $Er_{30}Lu_{10}$ sample.

non-magnetic constituent is independent of temperature. However, the results for Ho/Lu [6] superlattices are similar to those reported here. At high temperatures the wave-vector is 0.240 and q_{Lu} increases on cooling, in agreement with our results for Er/Lu superlattices.

Figure 7 shows the temperature dependence of the longitudinal amplitude A_c, and the ratio of the longitudinal and basal-plane moments, r, for the $Er_{30}Lu_{10}$ sample. The results for A_c show a steady increase with decreasing temperature following a curve similar to

a Brillouin function, while r shows a similar behaviour below T_N'. The low-temperature values of r are listed in table 3 for all the samples.

Finally, the centres of the magnetic scattering peaks observed for scans of the wave-vector transfer along $[0\,0\,l]$ and $[1\,0\,l]$ occur at positions corresponding to different phase shifts, Φ, across the SL blocks. This implies that the moments in the basal-plane do not have the same phase advance across the bilayers as for the c-axis moments. In the fits the wave-vectors of the scans were displaced to account for this and the differences in the phase shifts are listed for each sample in table 3. This difference is small, but if it is assumed that it arises from a different wave-vector for the longitudinal and basal-plane moments of the Er then the basal-plane turn angle would be smaller by up to 4°. A similar effect was observed for Er/Y SLs [3], and the effect will be discussed in section 4.

4. Discussion and summary

The results described in the previous section can be compared with those obtained for Er/Y SLs [3] and contrasted with those found for Ho/Y [4] and Ho/Lu [6] SLs. The Er wave-vector at the onset of magnetic ordering is very similar $(0.287 \pm 0.004)\boldsymbol{c}^*$, to that for bulk Er and for the SLs with both Y and Lu. This shows that the maximum of the exchange interaction, $J(q)$, is at this wave-vector for both the SLs and the bulk. Similarly the wave vector for the Lu is $0.241\boldsymbol{c}^*$ at the onset of magnetic ordering in agreement with that found for Ho/Lu alloys and SLs. Calculations [19] gave a peak in the conduction electron susceptibility of Lu at $0.267\boldsymbol{c}^*$, but we consider that the experimental value is to be preferred.

The magnetic transition temperatures of the superlattices tend to decrease with decreasing Er layer thickness. This is most likely because blocks of magnetic material of finite thickness have a lower transition temperature than bulk material.

The effect of strain on the transition temperatures can be estimated by using Landau theory. If the ordered moments are assumed to be plane waves in the a–c plane, the free energy for Er can be written as [20]

$$F - F_0 = A(T - T_c)(S_x^2 + S_z^2) + \tfrac{1}{2}gS_z^2 + \tfrac{3}{8}dS_z^4 + 3u(S_x^4 + S_z^4) + 2uS_x^2S_z^2 + \cdots$$

where S_x is the amplitude of the modulated moment in the x direction, $A(T - T_c)$ is the isotropic part of the inverse susceptibility, g and d are the anisotropic terms which are proportional to the difference between c/a and its ideal value $(8/3)^{1/2}$, and u is the interaction between the fluctuations due to the entropy and arises from the expansion of the Brillouin function. If $g < 0$, the transition temperature to a longitudinally modulated phase is given by

$$T_N = T_c - g/2A.$$

At a lower temperature, T_N', the basal-plane or x-components order where

$$T_N' = T_N + g(24u + 3d)/(2A(16u + 3d)).$$

The difference between c/a and the ideal value $(8/3)^{1/2}$, and the temperatures over which the longitudinally modulated phase is stable, T_N–T_N', are smallest for the Er/Lu SLs, larger for bulk Er and largest for Er/Y SLs. More quantitatively when T_N–T_N' is divided by the difference of the c/a-ratio from its ideal value the results for the SLs with thick layers of Er are 465, 508 and 469 K for Er/Y, bulk Er and Er/Lu SLs respectively. These are approximately constant showing that the changes in the temperature stability of the longitudinal phase result from the different strains of the SLs.

At low temperature, the Er/Lu SLs do not have the cone phase of bulk Er. The cone phase is stabilized by the dipolar forces and magneto-elastic contributions to the energy which only contribute if there is a long-wavelength component of the magnetic ordering, and by the anisotropy term described by g above. In the case of Er/Lu SLs, g is larger (less negative) than for bulk Er and so this term alone reduces the energy gain of a cone phase. Experiments by Beach *et al* [21] on Er films grown on Lu substrates suggest a rather more complicated behaviour. Thick films have a transition to a cone phase but on reducing the thickness to 800 Å the transition to a cone phase is suppressed, while on further reducing the thickness to below 600 Å the transition is restored. They did not investigate films as thin as those in our superlattices but these results clearly warrant further study. It is possibly also surprising that Er films grown on Y and Er/Y SLs do not have a cone phase although g is more negative for these materials than for bulk Er. This may be because the clamping of the basal-plane reduces the magnitude of the magneto-elastic contribution compared to that of bulk Er. Alternatively as discussed in the introduction, Andrianov [9] has suggested that there is a strong correlation between the wave-vector of the ordering and the ratio of c/a. This presumably arises from a correlation between changes in the c/a-ratio and the band structure and so a modulated magnetic structure may be energetically more favourable than a uniform structure.

There is considerably less temperature dependence to the wave-vectors q_{Er} and q_Y for Er/Y SLs [3] than for the corresponding wave-vectors for Er/Lu SLs. This is similar to the differences observed for Ho/Y [4] and Ho/Lu [6] SLs. Since there is little change of the ordering wave-vector in the longitudinally modulated phase of bulk Er, it is tempting to associate the changes with the development of basal-plane ordering. T_N' is much lower for Er/Y than for Er/Lu SLs and so the ordered basal-plane moment and the change in wave-vector with temperature are less for the Er/Y SLs. Additionally the peak of the conduction electron susceptibility of Lu is smaller and broader than for Y [19]. It is therefore easier for the wave-vector associated with the Lu layers to change than for that of the Y layers.

Finally there are two aspects of the properties of both Er/Y and Er/Lu SLs which are not understood. Firstly the coherence length decreases on cooling, as shown in figure 5, and secondly the longitudinal and basal-plane moments have different phase angles, Φ, across the bilayers. In the absence of spin–orbit coupling, the conduction electron wave-functions are symmetric in spin space, and there should be little difference in the way they respond to helical or cycloidal ordering. If, however, spin–orbit interaction is important the situation is more complex. In the longitudinally modulated phase a longitudinally modulated spin-density wave will be produced in the non-magnetic layer, and in the presence of spin–orbit interaction it will be difficult for this to become a cycloidal spin-density layer below T_N'. Consequently the development of basal-plane magnetic ordering will scatter the longitudinally polarized spin-density wave giving a shorter coherence length as the basal-plane moment increases. This is similar to the behaviour observed for Ho/Er superlattices [22].

It is more difficult to understand the difference of the phase angles of the basal-plane and longitudinally ordered moments, $\Delta\Phi$, which was observed for both Er/Y [3] and Er/Lu SLs. If the longitudinal and basal-plane moments become out of phase, this gives rise to an increase in the energy of the structure at low temperature. Possibly, as discussed above, the exchange interactions are different for the longitudinal and basal-plane moments and the correlation length, listed in table 3, is short enough that the gain in energy from the different wave-vectors is large enough to outweigh the loss in energy from the out-of-phase ordering over short distances. It is not easy to see how the introduction of trigonal terms can account for these results [11].

In conclusion we have studied the magnetic structures of Er/Lu SLs. There is a longitudinally modulated magnetic phase which on cooling becomes a cycloid which at low temperatures locks into a $\boldsymbol{q} = \frac{1}{4}\boldsymbol{c}^*$ commensurate cycloid in the Er layers. The cone phase found in bulk Er was not observed. Two features of the results which differ from those obtained for Ho/Lu SLs but which were also observed for Er/Y SLs [3] are a decreasing coherence length on cooling, and a different phase angle for the longitudinal and basal-plane magnetic ordering. The former possibly is the result of spin–orbit coupling on the conduction electron energy bands but the latter is not understood.

Acknowledgments

We are grateful to J Jensen and the late A R Mackintosh for discussions about these experiments and to the technical staff at Risø for their excellent support. EPSRC provided financial support at Oxford and a studentship for JAS, and the EU under the Large Installations Programme provided financial support at Risø.

References

[1] Erwin R W, Rhyne J J, Salamon M B, Borchers J, Sinha S, Du R, Cunningham J E and Flynn C P 1987 *Phys. Rev.* B **35** 6808
[2] Kwo J, Hong M, DiSalvo F J, Waszczak J V and Majkrzak C F 1987 *Phys. Rev. Lett.* **35** 7295
[3] Borchers J, Salamon M B, Erwin R W, Rhyne J J, Du R and Flynn C P 1991 *Phys. Rev.* B **43** 3123
[4] Jehan D A, McMorrow D F, Cowley R A, Wells M R, Ward R C C, Hagman N and Clausen K N 1993 *Phys. Rev.* B **48** 5594
[5] Beach R S, Borchers J A, Matheny A, Erwin R W, Salamon M B, Everitt B, Pettit K, Rhyne J J and Flynn C P 1993 *Phys. Rev. Lett.* **70** 3502
[6] Swaddling P P, McMorrow D F, Simpson J A, Wells M R, Ward R C C and Clausen K N 1993 *J. Phys.: Condens. Matter* **5** L481
[7] Yafet Y 1987 *J. Appl. Phys.* **61** 4058
[8] Wilkinson M K, Koehler W C, Wollan E O and Cable J W 1961 *J. Appl. Phys.* **32** 485
[9] Andrianov A V 1992 *JETP Lett.* **55** 666
[10] Cable J W, Wollan E O, Koehler W C and Wilkinson M K 1965 *Phys. Rev.* **140** A1896
[11] Cowley R A and Jensen J 1992 *J. Phys.: Condens. Matter* **4** 9673
[12] Gibbs D, Bohr J, Axe J D, Moncton D E and D'Amico K L 1986 *Phys. Rev.* B **34** 8182
[13] Rosen M, Kalir D and Klimker H 1973 *Phys. Rev.* B **8** 4399
[14] McMorrow D F, Swaddling P P, Cowley R A, Ward R C C and Wells M R 1996 *J. Phys.: Condens. Matter* **8** 6553
[15] Cooper M J and Nathans R 1967 *Acta Crystallogr.* **23** 357
[16] Helgesen G, Hill J P, Thurston T R, Gibbs D, Kwo J and Hong M 1996 *Phys. Rev.* B **50** 2990
[17] Cowley R A and Bates S 1988 *J. Phys. C: Solid State Phys.* **21** 4113
[18] Brown J 1983 *International Tables for Crystallography* vol C (Dordrecht)
[19] Liu S H, Gupta R P and Sinha S K 1971 *Phys. Rev.* B **4** 1100
[20] Jensen J and Mackintosh A R 1991 *Rare Earth Magnetism* (Oxford: Oxford University Press)
[21] Beach R S, Borchers J A, Erwin R W, Rhyne J J, Matheny A, Flynn C P and Salamon M B 1991 *J. Appl. Phys.* **69** 4535
[22] Simpson J A, Cowley R A, Jehan D A, Ward R C C, Wells M R, McMorrow D F, Thurston K N and Gibbs D 1996 *Z. Phys.* B **101** 35